Characterization and modelling of Langmuir interfaces with finite elasticity

Journal Article

Author(s):
Pepicelli, Martina; Verwijlen, Tom; Tervoort, Theo A. (iD); Vermant, Jan

Characterization and modelling of Langmuir interfaces with finite elasticity[†]

Martina Pepicelli,[a] **Tom Verwijlen,**[b] **Theo A. Tervoort,**[a] **and Jan Vermant**[*a]

Interfaces differ from bulk materials in many ways, one particular aspect is that they are compressible. Changing the area per molecule or per particle changes the thermodynamic state variables such as surface pressure. Yet, when compressing to high surface pressures, dense packing of the interfacial species induces phase transitions, with highly structured phases, which can display elastic or strongly viscoelastic behaviour. When these are deformed, in addition to the changes in the surface pressure, extra and deviatoric stresses can be induced. The traditional tool to study phase behaviour of monolayers is a rectangular Langmuir-Pockels trough, but as both area and shape of the interface are changed upon compression, the interfacial-strain field in this instrument is mixed with a priori unknown amounts of dilatational and shear deformations, making it difficult to separate the rheological and equilibrium thermodynamic effects. In the present work, the design of a radial trough is described, in which the deformation field is simple, purely dilation or compression. The possibility to now independently measure the compressional properties for different strains and the development of an appropriate finite strain constitutive model for elastic interfaces makes it possible to interrogate the underlying constitutive behaviour. This is shown here for a strongly elastic, soft glassy polymer monolayer during its initial compression but is easily generalised to many visco-elastic soft matter interfaces.

1 Introduction

The thermodynamic and rheological properties of interfaces play an important role in the stability of thin films or even the stability of macroscopic systems such as foams or emulsions[1–4]. Other areas of relevance include lung-surfactant replacements, which are used in neonatal therapy[5–9] or problems related to stability of tear films[10] or biofilms[11]. Like for bulk materials, interfacial rheology seeks to measure and describe rheological material functions, and link them to the underlying microstructures. However, as interfaces are compressible, in addition to the material functions for flows and deformations at constant area (such as shear and extensional flows), also the response to dilatational-compressional deformations needs to be measured and constitutively described.

Whereas an isotropic surface tension suffices for simple fluid-fluid interfaces, a surface-stress tensor which relates the surfaces stresses to strains is required when dealing with complex, structured fluid-fluid interfaces[3,5,12,13]. Hermans et al.[5] presented an approach where the role of the different material parameters and material functions are conceptually separated. This starts by writing the surface-stress tensor $\boldsymbol{\sigma}^s$ which is composed of an isotropic surface-tension contribution $\sigma_{\alpha\beta}(\Gamma)$, that depends on the surface concentration Γ of the surface-active component, and an extra stress $\boldsymbol{\sigma}^e$ of rheological origin, as shown in Equation 1[5,12].

$$\boldsymbol{\sigma}^s = \sigma_{\alpha\beta}(\Gamma)\mathbf{I} + \boldsymbol{\sigma}^e \tag{1}$$

When deforming an interface, the surface tension will generate forces related to capillarity when the curvature of the interfaces is changed. When the area is changed and Γ is varied, the compressibility (also called Gibbs elasticity)[4,14] comes into play, and further transport phenomena can play a role in the dynamics[15,16] as well as Marangoni stresses when the deformation of the interface entails gradients in concentration[11]. For structured interfaces with dense packings or lateral interaction between the surface active moieties, extra rheological stresses will resist changes in area and shape. The present work is mainly concerned with the effect of the latter on the measured isotherms.

Different methods have been proposed to determine the rheological material functions related to these extra rheological stresses. For the case of shear rheometry, several approaches and techniques have been developed and are commercially available[17–19]. For example, the magnetic rod

rheometer, the bi-cone geometry and the double-wall ring (DWR), all generate well defined kinematics with homogeneous shear deformations, provided the coupling between bulk and interfacial flows is accounted for[17–21]. Some of these methods can be combined with control of the surface concentration Γ, for example by compression[6,22], or by sub-phase exchange[23,24] . For extensional flows, 2D equivalents of the filament-stretching rheometer have been proposed[25], but here the situation is more complex, as mixed-flow fields occur and effects of compressibility, Marangoni stresses and rheological stresses have a complex interplay, making it difficult to deconvolute the different effects[26].

Similar difficulties of having mixed flow and deformation fields occur often in the case of dilatational-interfacial rheometry. For example, the deformation in a classical Langmuir-Pockels trough equipped with a Wilhelmy balance, which has been proposed as a rheometer, entails changes of both area and shape. This means that the interfacial-strain field utilised in this instrument is mixed, leading to an anisotropic state of stress that depends on the relative magnitudes of the compression and shear properties of the interface[27]. Only under certain circumstances, state variables and rheological parameters can be separated[12]. Aumaitre and coworkers have clearly shown the possible pitfalls of measuring rigid interfacial films using a Wilhelmy plate and a Langmuir trough[28]. Due to the anisotropic stress profile at the interface, variations of the trough width or of the Wilhelmy plate dimensions were found to influence the measured apparent isotherm in case of rigid films[28,29]. It has been shown that the measured isotherms depend on the surface coverage, but can not be readily rescaled by the area per molecule, as it would happen for a simple surface-tension measurement[28]. Furthermore, because of the presence of shear elasticity, by orientating the Wilhelmy probe with different directions compared to the compression axis, it is possible to distinguish shear from dilatational effects[27,30]. Nevertheless, obtaining a high degree of accuracy of the orientation of the Wilhelmy plate is non trivial.

Another widely used technique, the oscillating pendant drop, suffers from a similar complexity. These experiments are typically analysed by fitting the Young-Laplace (Y-L) equation to the drop shape. However, this fit will only work when the interfacial stresses are isotropic. When a system with a complex microstructure is present at the interface, extra and deviatoric stresses develop, which require the Y-L equation to be extended. Clear deviations of the drop shape, including even a wrinkling of the interface, are observed experimentally for a wide range of structured interfaces, in particular near the neck of the droplet[31–35]. To extract material properties, the Young-Laplace law needs to be generalised in order to account for extra anisotropic stresses and strains at the interface, as recently reviewed by Nagel et al.[36]. Variations of this method are the capillary-pressure tensiometer (CPT) and the pulsating-bubble surfactometer (PBS)[37,38]. Both methods couple a shape analysis with a pressure measurement, using generally smaller capillaries to increase the pressure signal. The shape analysis simplifies considerably when the capillary pressure is provided, because only the curvature has to be determined. Still, the curvature is constant but the strains in different directions are generally not equal as discussed by Nagel et al.[36].

In many applications, ranging from food industries, coating and paints, to medical applications, the scale of deformation to which elastic or highly viscoelastic interfaces are subjected to, can be large[1–4]. The present work focuses on the development of adequate finite-strain constitutive models. As a first step towards general viscoelastic models, we focus on neo-Hookean models (and materials) that use linear-elastic material parameters combined with appropriate strain measures to describe large elastic deformations. Similarly to bulk rheology, these so-called quasi-linear elastic models are a stepping stone for more advanced viscoelastic and non-linear rheological models. Such a model is characterised by frame invariant and objective strain measures which measure relative deformations, with the material being characterised by constant parameters, as is done in bulk rheology[13]. The peculiarity of interfaces is that now the compressibility comes into play and moreover extra dilatational stresses need to be dealt with. We focus on finite elastic deformations of the interface. As a continuum approach is pursued, the interface is assumed to be "sharp", and all effects can be described by considering the interfacial effects through a stress boundary condition. Such a stress boundary condition for elastic interfaces can be used to deconvolute the effects of compressibility and the extra and deviatoric stresses occurring in a Langmuir through.

Experimentally, a first difficulty in determining accurate material functions lies in the mixed deformation fields that often occur, especially in dilatational-interfacial rheometry, as mentioned above. In order to avoid shear contributions and to be able to apply a large-scale pure dilatational deformation, a more symmetric area change is required. This was achieved in earlier works to some extent by the development of adapted versions of the Langmuir trough with radial symmetry. However, these designs have only been used for some restricted case studies. Abraham and coworkers, for example, developed an apparatus consisting of a Teflon cup that enables an isotropic compression of the interface by simultaneously withdrawing the bulk fluid while rising the cup[39]. The drawbacks of such technique are that the compression ratio is limited, a complex fluid mechanical analysis will be required

for rheological measurements at finite deformation rates and the possible leakage and issues with adsorption onto the walls. To overcome these problems, Miyano and Maeda built a new type of trough, consisting of four independently movable barriers, such that an interface can be purely sheared or purely dilated[40]. Nevertheless, in presence of elastic interfaces, even if operated in pure dilation/compression mode, this set-up can induce shear effects due to sticking of material to the barriers. In order to overcome these limitations Bohanon and coworkers designed an apparatus able to isotropically compress and stretch the interface using an elastic barrier[41]. Lastly, Matsumoto and coworkers obtained a radial compression and deposition of a monolayer, by the compression of twenty thin blades mimicking the mechanism of an iris diaphragm[42]. In the present work we introduce a new radial trough with an improved mechanical design, similar in spirit to the one presented by Bohanon and coworkers.

A second difficulty in dealing with compressional rheology lies in the fact that the changes in the isotropic parts of both the first and second term in eqn. 1 cannot be easily separated[12]. We therefore selected a model compound, poly(ter-butyl methacry-late) (PtBMA) at an air-water interface, which we deform upon its initial compression run. The structure obtained after spreading is highly visco-elastic and we deform it at rates corresponding to a sufficiently high Deborah number, conditions chosen to be such that strong elastic effects are present and significant extra and deviatoric stresses are expected to occur. The strain will be measured in compression from the first moment that the sample becomes elastic. A prime objective of the present work is to experimentally evaluate the derived quasi linear models. At the same time this will be of use to evaluate to what extent rheological effects influence the measurements of isotherms in a Langmuir through and it is also an important building block towards models for viscoelastic interfacial rheology.

2 Theory

Upon the introduction of a surface-active compound to an interface between two phases, the constant surface stress of the clean interface becomes a function of the equilibrium concentration Γ of the surface active component on the surface, typically expressed in area per monomer. Depending on the surface concentration of the surface-active compound, the surface stress can then become a function of the deformation of the interface. In the absence of surface bending forces, this surface stress due to deformation of an interface is usually characterised by the extra surface-stress tensor $\boldsymbol{\sigma}^e$, related to the total surface-stress tensor $\boldsymbol{\sigma}^s$ as:

$$\boldsymbol{\sigma}^e = \boldsymbol{\sigma}^s - \sigma_{\alpha\beta}(\Gamma)\mathbf{I} \qquad (2)$$

Here, $\sigma_{\alpha\beta}(\Gamma)$ is the surface tension between phases α and β in dependence of the equilibrium concentration of the surface-active component Γ, and $\mathbf{I}$ is the unit tensor on the surface[2,12]. It should be noted that $\boldsymbol{\sigma}^e$ can contain both an isotropic and a deviatoric part.

In this work, the focus is on finite elastic deformations of the interface, characterised by the 2-dimensional surface-deformation gradient tensor $\mathbf{F}^s = \partial\mathbf{r}/\partial\mathbf{R}$, where $\mathbf{r}$ and $\mathbf{R}$ are the position vectors in the deformed and reference configuration, respectively. Small-strain[27] and "hypoelastic" finite-strain[12] constitutive relations for surface-elastic deformations have been proposed proposed before. There is a clear need to go beyond the small deformation regime, but the constitutive model by Verwijlen et al.[12] was not material-frame indifferent. Whereas this was not a problem in their subsequent 1D analysis of the Langmuir trough, this will lead to incorrect results for large area deformations in general, as was recently pointed out by Balemans et al.[43]. In what follows, finite "hyperelastic" relations will be derived that are rigorously derived from a strain-energy function[44].

In what follows, all extra surface stresses and surface strains are supposed to be fully elastic. Upon an arbitrary surface deformation, the eigenvalues of $\mathbf{F}^s$ are the two principal stretches λ_1 and λ_2, defined as $\lambda_1 = L_1/L_1^0$ and $\lambda_2 = L_2/L_2^0$, where L_i^0 and L_i are the edges of a part of the surface in the reference -and deformed state, respectively (see Figure 1).
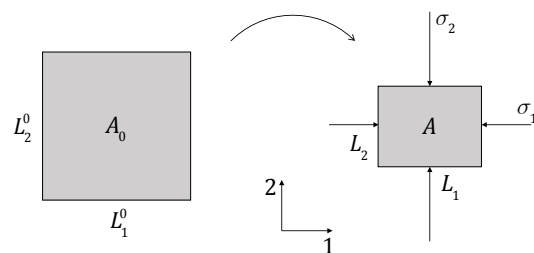

Fig. 1 Schematic drawing of the *elastic* surface deformation in the principle-strain directions, showing the undeformed reference state with edges L_i^0 and the deformed state with edges L_i and principle Cauchy extra stresses (force per unit deformed line) σ_i^e.

Referring to Figure 1, the principal extra nominal stresses, i.e. the so-called Biot stresses t_i, are defined as the forces (F_1 and F_2) per unit undeformed length as:

$$t_1 = \frac{F_1}{L_2^0} \qquad \text{and} \qquad t_2 = \frac{F_2}{L_1^0} \qquad (3)$$

The principle extra true surface stresses, i.e. the Cauchy stresses σ_i, are defined as the forces per unit deformed length and are related to the nominal stresses t_i as:

$$\sigma_1 = \frac{F_1}{L_2} = \frac{F_1}{\lambda_2 L_2^0} = \frac{t_1}{\lambda_2} \qquad (4a)$$

$$\sigma_2 = \frac{F_2}{L_1} = \frac{F_2}{\lambda_1 L_1^0} = \frac{t_2}{\lambda_1} \qquad (4b)$$

which can be written as:

$$J\sigma_1 = \lambda_1 t_1 \quad \text{and} \quad J\sigma_2 = \lambda_2 t_2 \qquad (5)$$

Here, J is the relative area deformation given by (see Figure 1):

$$J = \frac{A}{A_0} = \lambda_1 \lambda_2 = \det(\mathbf{F}^s) \qquad (6)$$

The set of principle stretches (λ_1, λ_2) completely describes the applied elastic surface deformation. Following Ogden[45], to derive constitutive equations for finite elastic surface deformations, it is now assumed that at constant temperature, a strain energy function $a(\lambda_1, \lambda_2)$ with respect to the undeformed configuration exists, such that:

$$t_1 = \frac{\partial a(\lambda_1, \lambda_2)}{\partial \lambda_1} \quad \text{and} \quad t_2 = \frac{\partial a(\lambda_1, \lambda_2)}{\partial \lambda_2} \qquad (7)$$

with the requirement that in the reference state $a(1,1) = 0$.

To separate the deformation in a surface dilatational and a distortional part, modified stretches λ_i^* are introduced as:

$$\lambda_1^* = \frac{\lambda_1}{\sqrt{J}} = \sqrt{\frac{\lambda_1}{\lambda_2}} \quad \text{and}$$

$$\lambda_2^* = \frac{\lambda_2}{\sqrt{J}} = \sqrt{\frac{\lambda_2}{\lambda_1}} \qquad (8)$$

so that:

$$\lambda_1^* \lambda_2^* = 1 \qquad (9)$$

As only one of the modified stretches is independent, the elastic deformation can also be described by the set (λ_1^*, J), which implies that the strain energy can be written as: $\hat{a}(\lambda_1^*, J) \equiv a(\lambda_1, \lambda_2)$. This, combined with Equation (7), gives:

$$\frac{\partial \hat{a}(\lambda_1^*, J)}{\partial \lambda_1^*} d\lambda_1^* + \frac{\partial \hat{a}(\lambda_1^*, J)}{\partial J} dJ$$
$$= \frac{\partial a(\lambda_1, \lambda_2)}{\partial \lambda_1} d\lambda_1 + \frac{\partial a(\lambda_1, \lambda_2)}{\partial \lambda_2} d\lambda_2 \qquad (10)$$
$$= t_1 d\lambda_1 + t_2 d\lambda_2$$

Combining Equations 5, 6 and 10 then leads to:

$$J(\sigma_1 - \sigma_2) = \lambda_1^* \left(\frac{\partial \hat{a}}{\partial \lambda_1^*} \right) = \left(\frac{\partial \hat{a}}{\partial \ln \lambda_1^*} \right) \qquad (11)$$

and for the isotropic part of $\boldsymbol{\sigma}^e$, σ_{iso}^e:

$$\frac{(\sigma_1 + \sigma_2)}{2} = \sigma_{\text{iso}}^e = \left(\frac{\partial \hat{a}}{\partial J} \right) = \frac{1}{J} \left(\frac{\partial \hat{a}}{\partial \ln J} \right) \qquad (12)$$

Equations (11) and (12) suggest to use the set of logarithmic Hencky strain measures, $(\ln \lambda_1^*, \ln J)$, as independent variables, as it is known that substitution of Hencky strains for linear strains is an efficient way to incorporate moderate strain nonlinearities[46]. A logical choice for $\hat{a}$ that is quadratic in $\ln \lambda_1^*$ and $\ln J$ and in the limit of small strains reduces to the familiar equations of linear elasticity with the surface shear modulus G and surface dilatational modulus K, is:

$$\hat{a} = 2G(\ln \lambda_1^*)^2 + \frac{K}{2}(\ln J)^2 \qquad (13)$$

Applying Equations (11) and (12), then leads to the first constitutive equation:

$$\sigma_1 - \sigma_2 = \frac{4G}{J} \ln \lambda_1^*$$
$$= \frac{4G}{J} \ln\left(\sqrt{\frac{\lambda_1}{\lambda_2}} \right) = \frac{2G}{J} \ln\left(\frac{\lambda_1}{\lambda_2} \right) \qquad (14a)$$

$$\frac{\sigma_1 + \sigma_2}{2} = \frac{K}{J} \ln J \qquad (14b)$$

As an alternative to the set of principle stretches to describe the elastic-surface deformation, the surface-deformation gradient tensor itself can be used to construct finite strain tensors. In the case of isotropic elastic behaviour, a convenient choice is the left-Cauchy-Green surface strain tensor, $\mathbf{B}^s = \mathbf{F}^s \mathbf{F}^{s,T}$, where $\mathbf{F}^{s,T}$ is the transpose of $\mathbf{F}^s$. To separate distortional from area deformation, a left-Cauchy-Green surface-strain tensor at constant area, $\tilde{\mathbf{B}}^s$, can be defined to characterise the distortional deformation as[47]:

$$\tilde{\mathbf{B}}^s = \frac{\mathbf{B}^s}{J} \qquad (15)$$

In principle-strain space, the components of $\tilde{\mathbf{B}}^s$ then become:

$$\tilde{B}_{ij} = \begin{pmatrix} \lambda_1^{*2} & 0 \\ 0 & \lambda_2^{*2} \end{pmatrix} = \begin{pmatrix} \lambda_1^{*2} & 0 \\ 0 & \frac{1}{\lambda_1^{*2}} \end{pmatrix} \qquad (16)$$

Using $\tilde{\mathbf{B}}^s$, the set of variables to describe surface-elastic deformation becomes $(\tilde{\mathbf{B}}^s, J)$. An alternative expression to Equation (10) for the distortional part of the strain energy, that is linear in $\tilde{\mathbf{B}}^s$, then involves the first invariant (the trace) of $\tilde{\mathbf{B}}^{s}$ [47]:

$$
\begin{aligned}
\hat{a} &= \frac{G}{2} \operatorname{Tr}\left(\tilde{\mathbf{B}}^s - \mathbf{I}\right) + \frac{K}{2}(\ln J)^2 \\
&= \frac{G}{2}\left(\lambda_1^{*2} + \frac{1}{\lambda_1^{*2}} - 2\right) + \frac{K}{2}(\ln J)^2
\end{aligned}
\tag{17}
$$

As before, this strain energy expression becomes zero in the absence of deformation and converges to linear elasticity in the small-strain limit. Applying Equations (11) and (12) then leads to a second, "Neo-Hookean," constitutive equation for finite surface elasticity:

$$
\begin{aligned}
\sigma_1 - \sigma_2 &= \frac{G}{J}\left(\lambda_1^{*2} - \frac{1}{\lambda_1^{*2}}\right) \\
&= G\left(\frac{1}{\lambda_2^2} - \frac{1}{\lambda_1^2}\right)
\end{aligned}
\tag{18a}
$$

$$
\frac{\sigma_1 + \sigma_2}{2} = \frac{K}{J}\ln J = \frac{K}{\lambda_1 \lambda_2}\ln\left(\lambda_1 \lambda_2\right)
\tag{18b}
$$

The "Neo-Hookean" constitutive equation can also be written as a coordinate-free tensor relation as:

$$
\boldsymbol{\sigma}^e = \frac{K}{J}\ln(J)\mathbf{I} + \frac{G}{J}\left(\tilde{\mathbf{B}}^s - \frac{1}{2}\operatorname{Tr}\left(\tilde{\mathbf{B}}^s\right)\mathbf{I}\right)
\tag{19}
$$

For the Hencky-strain constitutive model, the tensor formulation involves coefficients that are a function of the principle strains [48], and is, hence, less useful.

In case of compressing an elastic interface in a rectangular Langmuir trough, deformation in the perpendicular direction is constrained, so that the principle stretches are $\lambda_1 = A/A_0 = \lambda$ and $\lambda_2 = 1$, see Figure 5. The corresponding principle Cauchy stresses, σ_1 and σ_2, follow directly from the constitutive equations (14) or (18) and can be measured experimentally by two Wilhelmy plates, positioned parallel (σ_1) and orthogonal (σ_2) to the barriers [27] (see Section 4.1).

For the "Hencky-strain" constitutive relation (Equation 14), the principle stresses then become:

$$
\sigma_1 = (K+G)\frac{\ln\lambda}{\lambda}
\tag{20a}
$$

$$
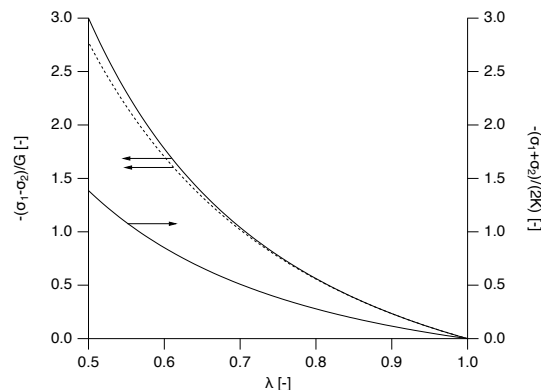\sigma_2 = (K-G)\frac{\ln\lambda}{\lambda}
\tag{20b}
$$

Fig. 2 Plots of the (negative) normalised normal-stress difference $-(\sigma_1 - \sigma_2)/G$ (left axis) -and hydrostatic stress $-(\sigma_1 + \sigma_2)/(2K)$ (right axis) for both the "Hencky" Eq. (20) (dashed line) -and the "Neo-Hookean" constitutive equation Eq.(21) (solid lines) in a rectangular Langmuir trough as a function of λ $(= A/A_0)$. The hydrostatic stress response is identical for both models.

For the "Neo-Hookean" constitutive relation (Equation 18), the following expression for the principle stresses is found:

$$
\sigma_1 = \frac{G}{2}\left(1 - \frac{1}{\lambda^2}\right) + K\frac{\ln\lambda}{\lambda}
\tag{21a}
$$

$$
\sigma_2 = \frac{-G}{2}\left(1 - \frac{1}{\lambda^2}\right) + K\frac{\ln\lambda}{\lambda}
\tag{21b}
$$

Figure 2 shows for both the "Hencky" Eq.(20) -and the "Neo-Hookean" constitutive equation Eq.(21) a plot of the normalised normal-stress difference $(\sigma_1 - \sigma_2)/G$ and normalised hydrostatic stress $(\sigma_1 + \sigma_2)/(2K)$ (which is the same for both models) as a function of λ. From this figure, it can be seen that for the rectangular Langmuir trough configuration, the difference between both constitutive equations is rather small for deformations up to 50% compression.

In case of pure shear deformation, the area is per definition constant, leading to zero "hydrostatic" stress for both models. A plot of the normalised normal-stress difference for both models is shown in Figure 3. Again, for moderate deformations up to a shear strain $\gamma = 2$, the response is similar. For larger deformations, the normal-stress difference for both models diverge. The normalised shear stress τ/G for both models is also depicted in Figure 3. The shear response for both models is again identical for moderate shear strains, but for large shear deformations, the shear stress according to the Hencky model depicts a maximum, which is considered to be physically unrealistic [12].
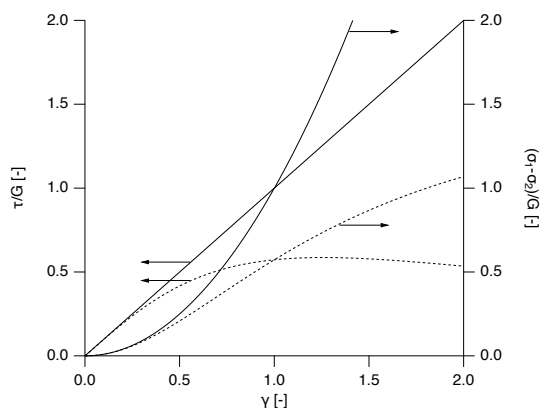
Fig. 3 Plots of the normalised shear stress τ/G (left axis) and normal-stress difference $(\sigma_1 - \sigma_2)/G$ (right axis) for both the "Hencky" Eq. (20) (dashed lines) -and the "Neo-Hookean" constitutive equation Eq.(21) (solid lines) as a function of shear strain γ.

In case of elastic surface deformation in the radial trough, see Figure 4, the deformation is homogeneous and isotropic, meaning that everywhere $\lambda_1 = \lambda_2$ (see also Section 3.2). From this it follows immediately that $\lambda_1^* = 1$ and from Equation (11) and (12) that $\sigma_1 = \sigma_2 = \sigma_e^{\text{iso}}$. The isotropic response is equal for both the Hencky and Neo-Hookean strain energy expressions, Equations (10) and (17), so that for both cases the extra stress is given by:

$$\sigma_1 = \sigma_2 = \sigma_e^{\text{iso}} = K \frac{\ln(J)}{J} \tag{22}$$

However, note that for the radial trough $J = \lambda^2$ and for the rectangular Langmuir trough $J = \lambda$.

In the above, it was shown that the difference between the two constitutive equations derived in this section, the Hencky-strain -and the Neo-Hookean model, is small at modest deformations. It was also found that it is possible to formulate the Neo-Hookean equation in a compact coordinate-free tensor form, which is convenient for implementation in finite-element codes. For these reasons, in what follows below, only the Neo-Hookean model will be verified experimentally, with the understanding that the Hencky-strain model, using the same experimental values of K and G, will perform equally well for the range of deformations applied in this study.

3 Materials and methods

3.1 Mechanical design

A custom-made radial trough setup was designed, shown in Figure 4. An elastic barrier is used to control the radial compression. It is made of poly(styrene-butadiene-styrene,

SBS) fabricated by Vreeberg BV (Nijkerk, The Netherlands). It is held in place by twelve aluminium fingers that move on individual rails. The maximum compression ratio achievable is $A_{max}/A_{min} = 4$. In principle, three fingers would be sufficient to apply a uniform deformation if a triangular shape is maintained, but to facilitate the fluid mechanics analysis, radial symmetry is preferred. A stepper motor (A-LST0250A, Zaber, US) controls the motion and the speed of the elastic barrier. Each finger is connected to the motor by ultra-high molecular weight polyethylene wires (UHMWPE, Dyneema®). These wires run on individual aluminium screws to allow a smooth movement of the fingers. Twelve adjustment bolts enable one to control the tension in the wires and two to tighten the individual wires during the calibration procedure, similarly to a guitar tuning.

The stepper motor has a step size of 0.124 micron, a travel range of 25.4 cm and a variable speed between 0.0012 and 22 mm/s with a resolution of 0.0012 mm/s. The maximum continuous thrust is 560 N, which is sufficient to stretch the elastic barrier. The motor is programmed using JavaScript to apply sinusoidal area changes or continuous compression and expansions. During compression, the elastic restoring force of the elastic barrier is not sufficient, but this is assured by a system of springs mounted below the base plate.

The trough itself is made from Teflon®, with an outer diameter of 25 cm and an inner diameter of 20 cm. Along the circumference of the trough, a sharp edge is present to ensure pinning of the interface, and a height of 1 cm above and below for the lower and upper liquid phases. The surface tension is measured using a Wilhelmy balance with a platinum rod to maintain the radial symmetry or using microtensiometers, of which the deflection can be detected by an optical train system as shown in Figure 4[49,50]. Temperature control is ensured by an aluminium heat exchanger below the Teflon trough, connected to an external water bath. Figure 4 shows that the entire apparatus is enclosed in a custom-made chamber that allows for humidity and temperature control, positioned on a vibration-isolation system (Halcyonics Vario Basic, Accurion GmbH).

The 12 fingers have Teflon-coated tips, and a position mechanism has been designed such that they can move vertically, without changing their radial position, as highlighted by the red arrow in Figure 4. This facilitates the correct positioning of the elastic barrier at the interface and the removal of the trough for cleaning purposes.
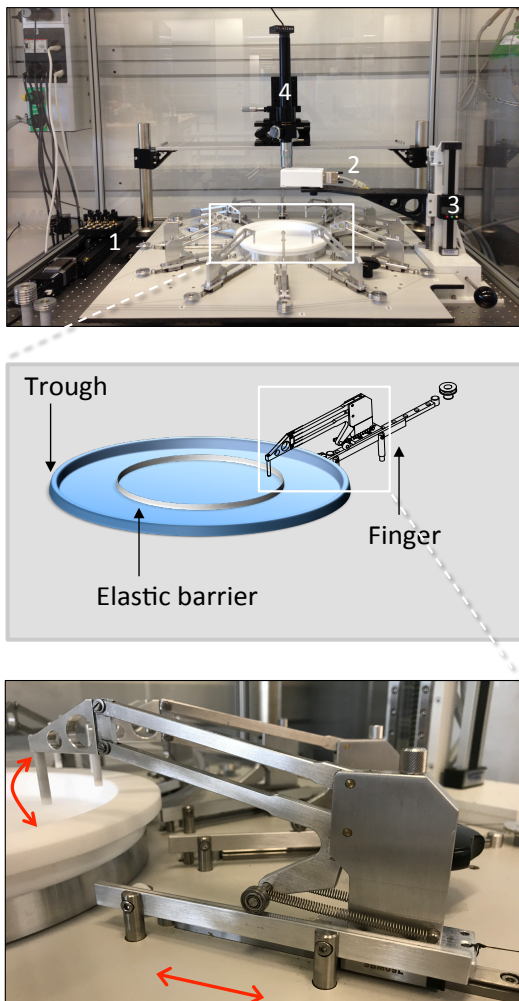
Fig. 4 Schematic of the radial trhough setup composed of a circular Teflon trough with an elastic barrier and 12 aluminium fingers, controlled by a stepper motor (1). The Wilhelmy balance (2) is positioned on a micro-positioner stage (3). In addition, the interface can be visualised using an optical system (4) mounted on a moving platform. The expanded illustration shows the working principle of the elastic barrier and the fingers.

3.2 Homogeneity of the deformation

The radial symmetry enables a homogeneous deformation, and for quasi-static measurements, a pure compression / dilation is ensured. In polar coordinates the deformation in the radial trough is given by:

$$r = r(R) \tag{23}$$

$$\theta = \Theta \tag{24}$$

The capital letters and indices refer to the reference configuration and small letters and indices to the deformed configuration. The dyadic form of the deformation gradient for the radial trough then follows in polar coordinates as:

$$
\begin{aligned}
\mathbf{F} &= \frac{\partial \mathbf{r}}{\partial \mathbf{R}} = \mathbf{r} \overleftarrow{\nabla}_{\mathbf{R}} \\
&= r(R)\mathbf{e}_r \left(\frac{\overleftarrow{\partial}}{\partial R} \mathbf{e}_R + \frac{\overleftarrow{\partial}}{\partial \Theta} \frac{1}{R} \mathbf{e}_\Theta \right) \\
&= r'(R)\mathbf{e}_r\mathbf{e}_R + \frac{r(R)}{R}\mathbf{e}_\theta\mathbf{e}_\Theta
\end{aligned}
\tag{25}
$$

Or, in matrix form:

$$
F_{iJ} = \begin{bmatrix} r'(R) & 0 \\ 0 & \frac{r(R)}{R} \end{bmatrix}
\tag{26}
$$

where $r'(R)$ is $\frac{\partial r(R)}{\partial R}$. The quantities $r(R)$ and $r'(R)$ are unknown beforehand. However, the relative-area deformation A/A_0 is equal to the determinant of F_{iJ}. Assuming that the material is isotropic, the relative-area deformation A/A_0 is only determined by the isotropic part of the stress. Moreover, it follows from the boundary conditions that the isotropic stress is constant throughout the radial trough, which implies that also the determinant of F_{iJ} is constant and thus independent of R:

$$
\begin{aligned}
\frac{\partial \det(F_{iJ})}{R} &= \frac{\partial \left(\frac{r'(R)r(R)}{R} \right)}{\partial R} \\
&= \frac{Rr'(R)^2 + r(R)(Rr''(R) - r'(R))}{R^2} = 0
\end{aligned}
\tag{27}
$$

This differential equation has the following positive solutions:

$$r(R) = c_2\sqrt{c_1 + R^2} \tag{28}$$

In the centre of the radial trough, $r(0) = 0$, and a point on the edge $R = R_0$ will transform to $r(R_0) = r_e$, as schematically depicted in Figure 5.

Substitution of these boundary conditions then gives:

$$r(R) = \frac{r_e}{R_0}R = \lambda R \tag{29}$$

With the imposed deformation $\lambda = r_e/R_0$. Substitution of Equation 29 in Equation 26 then results in the familiar form of the (constant) deformation gradient given as:

$$
F_{iJ} = \begin{bmatrix} \lambda & 0 \\ 0 & \lambda \end{bmatrix}
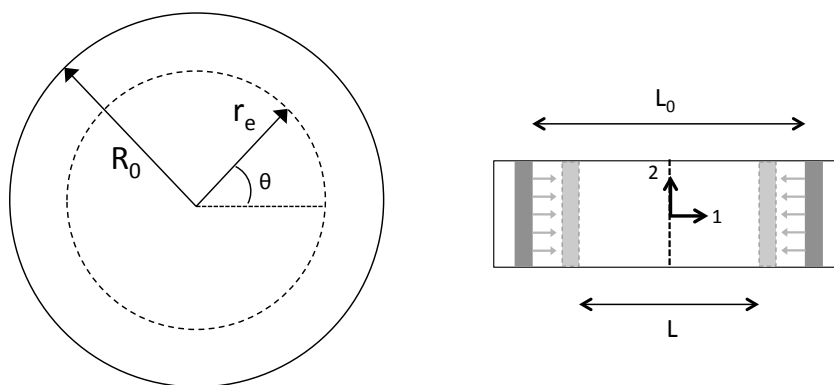\tag{30}
$$

Fig. 5 Left: Geometry of the radial trough for the analysis of the homogeneous deformation. $R = R_0$ is the radius before the deformation, while $r(R_0) = r_e$ is the corrisponding radius after an homogeneous compression. Right: Schematic drawing of a Langmuir trough, showing the principle-stretch directions "1" and "2".

3.3 General : Sample preparation

Poly(tert-butyl methacry-late) (PtBMA, Sigma-Aldrich, weight-average molar mass M_w = 170 kg mol^{-1}) spread at an air-water interface was chosen as a good water-insoluble model system. It belongs to the class of acrylic polymers that are well characterised in literature[51–53]. Their bulk glass transition temperatures ($\sim$ 112°C,[54]) are far above the room temperature and once deposited on a air water interface they exhibit a soft glassy behaviour, similar to other glassy polymers[53]. For such glassy polymers the polymer chains at the overlap concentration act as densely packed soft particles, eventually packing in multilayers with strong elastic responses[51,53]. The rheological properties of such systems can be described by the soft glassy rheology model of Sollich et al.[55]. When this interface is deformed faster than it can relax it can be expected to react elastically.

Solutions of PtBMA in chloroform were prepared at concentrations that varied from 0.1 to 0.3 mg/ml to ensure a reproducible spreading at the interface. The solutions were added drop-wise to the fluid interface using a 50 μl glass syringe (Hamilton Company, USA), following sonication of the sample for 30 min in cold water (4°C) to avoid chloroform evaporation. The interface was allowed to equilibrate for 45 minutes prior to the start of each measurement.

3.4 Continuous and stepwise compressions at an air-water interface

Pressure-area "isotherms" were measured in a standard rectangular Langmuir trough (7.5 x 32.2 cm internal area, KSV-NIMA, Finland), as well as in the custom-made radial trough described earlier. The surface pressure Π was measured in the rectangular trough using a platinum Wilhelmy plate (wetted length 39.44 mm, KSV-NIMA, Finland) and in the radial trough with a platinum rod (1.05 mm diameter, KSV-NIMA, Finland) to keep the radial symmetry.

In order to compare the compression measurements performed with the different geometries, an initial surface coverage of 0.778 mg/m^2 was used in all cases. The barier speed was set to 3 mm/min (rectangular trough) and 1.5 mm/min (radial trough) to ensure comparable compression rates. In addition to the curves obtained during continuous compression, stepwise experiments were performed in which the active compression was stopped and the decay of the surface pressure with time was recorded, until all transient stresses had relaxed.

To obtain reproducible experiments, careful cleaning is required. Before each measurement, the tips of the 12 fingers and the Teflon trough were cleaned using acetone, ethanol and rinsed with de-ionized water (Millipore MilliQ system, resistivity 18.2 MΩ.cm). The elastic bands were stored in MilliQ water and, when needed, they were cleaned following the same procedure as for the trough. To maintain

proper elastic properties, the bands were never used more than 4 times. All experiments were conducted at 23±0.5°C and the temperature at the interface was monitored using a thermocouple (NI USB-TC01, National Instruments, USA).

3.5 Interfacial shear rheology at controlled surface pressures

Interfacial shear rheology measurements were conducted using a stress-controlled rheometer (DHR-3, TA instruments) equipped with a double wall ring (DWR) geometry [19]. To allow measurements of rheological properties at variable surface pressure, an open Teflon cup was placed into a Langmuir trough and the DWR positioned at the enclosed interface [6,19]. During the shear experiments, the surface pressure was monitored using a Wilhelmy balance (as illustrated in the Supplementary Information, Figure S.3.). Frequency sweeps were performed at compressions corresponding to five different areas per molecule (12, 13, 14, 15, 17, 19 and 22 Å²/molecule) in the linear viscoelastic regime at a strain amplitude of 1%. In order to determine the linear viscoelastic regime, amplitude sweep at an area per molecule of 10 and 12 Å² and at a frequency of 1 rad/s were measured, showing a critical strain amplitude of around 3 %. In between subsequent compression experiments, the interface was allowed to equilibrate for about 15 minutes.

4 Experimental results and discussion

4.1 Compression experiments

Commonly, compression experiments in Langmuir troughs are associated with the study of equilibrium properties, the so-called isotherms, in reference to the intention to measure the state variables. Such measurements elucidate the relation between surface coverage of insoluble monolayers and its resulting surface tension. However, rheological effects, in particular the formation of elastic structures, have been shown to influence the measured stress [12]. Nevertheless, this is often neglected, although clear accounts of possible problems have been given for a wide range of materials [12,28,56]. In the present work we first explore how, when and if viscoelastic effects also come into play.

As shown in Equation 1 the surface-stress tensor σ^s includes also an extra component σ^e that can be deviatoric in nature. If this is the case, a Wilhelmy plate placed in the centre of a rectangular trough will measure different stress responses depending on its orientation compared to the compression axis [27,56]. Figure 6 illustrates the experimentally observable apparent isotherms, Π_a, of PtBMA as recorded in the radial
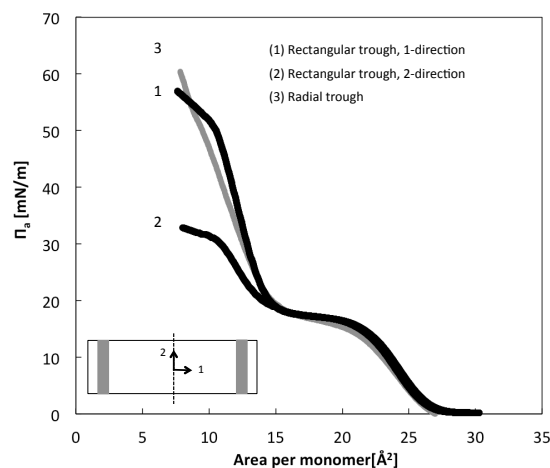
Fig. 6 Apparent surface pressure versus area per monomer of PtBMA using both a radial trough (Wilhelmy rod, curve 3) and rectangular Langmuir trough (Wilhelmy plate, curve 1 and 2). The small inset schematic shows the two principal orientations in the rectangular trough, 1-direction (corresponding to curve 1, as measured by a Wilhelmy plate parallel to the barriers) and 2-direction (corresponding to curve 2, as measured by a Wilhelmy plate orthogonal to the barriers).

trough using the Wilhelmy rod (1), and in the rectangular trough using a platinum Wilhelmy plate positioned parallel (2) and orthogonal (3) to the barriers.

PtBMA isotherms show a well-defined plateau at a surface pressure of 18 mN/m that marks the transition from a uniform monolayer to the formation of a second layer or a flipping of the molecules [51]. The projected area of a molecule of PtBMA in its planar configuration (lying flat at the interface) was shown to be approximately 23 Å², which coincides to the point in the apparent isotherms where this first plateau region starts. A second plateau is observed around a surface pressure of 55 mN/m for the rectangular trough with a parallel plate orientation. In literature, this higher plateau is generally explained by the complete filling of the second layer and the start of additional layer formation [57,58]. In contrast, the apparent isotherm measured in the exact same rectangular trough, yet with orthogonal plate orientation, shows a second plateau at much lower value in surface pressure, approximately around 30 mN/m. After the second plateau, the experimental measured surface pressure in the radial through lies between the two apparent surface pressures in the rectangular through, indicating that the deviatoric stress contribution in the Langmuir trough either increases or decreases the surface pressure with respect to the isotropic value. Interestingly, at high compressions the curve measured in the radial though does not show any sign of a second plateau, most probably because

of the more uniform deformation applied.

Up to compressions of an area per molecule of approximately 15 Å^2 all curves overlay one another, while for higher compression ratios they clearly deviate as the layer becomes structured and extra and deviatoric stresses develop. For thermodynamic state variables, such as the surface tension, all the curves should fall onto a unique master curve; at constant temperature the state variable should only depend on surface concentration. More specifically, in the regions where rheological effects, σ^e, can be neglected compared to the thermodynamic response $\sigma_{\alpha\beta}(\Gamma)$, the geometry of the measuring system does not have an influence, as expected. Conversely, once the interfacial layer starts to becomes structured and (visco)elastic and the associated extra stress σ^e predominant, a combination of the two responses is measured, explaining the disagreement of the three curves for high compression ratios. Even though the rheological effects can potentially be neglected for phase-transition studies limited to the liquid regime, extra and deviatoric stresses will be present and intermingled with the compressibility term. This last result is particularly important when using a Langmuir trough apparatus for the determination of rheological material functions. In this respect, the radial trough offers an advantage in applying a pure dilatational deformation without shear deformations. At sufficiently high Boussinesq numbers, the deformation by the barriers is nicely transmitted to the interface and a homogeneous compression is obtained.

4.2 Elastic effects during compression

When using a Langmuir trough to measure an equilibrium property such as surface pressure as a function of surface coverage, theoretically, one should apply an infinitely slow compression speed. Nevertheless, for practical reasons, these speeds are maintained to finite values, sufficiently slow so that they do not influence the measured surface pressure. In case of PtBMA the speed range that can be used lies between 1 mm/min and 7 mm/min. It is worthwhile to mention that no matter how slow the compression is, when the interfacial layer becomes elastic the relaxation time of the layer diverges to infinity. Even before that, there will be a point where the inverse of this relaxation time will be on the same order as the compression rate. For this reason a stepwise compression measurement with intermediate relaxations was performed. This method will enhance the difference between an "equilibrium" measurement that comes closer to the thermodynamic property (although it may include static elastic effects) and a continuous experiment that unavoidably, at some point, will detect a combination of dynamic and static properties.

In Figure 7 (A) the apparent surface pressures obtained using the radial through continuous compression at a speed of 1.5 mm/min (black solid line) are compared with data obtained upon successive compression/relaxation experiments, where the apparent surface pressure is allowed to relax to an equilibrium value (coloured symbols). Once the first plateau at 18 mN/m has been reached, and more specifically at areas per monomer below 15 Å^2, the two experiments start to diverge from each other. This deviation occurs as the time scale associated with the compression becomes shorter than the time it takes to relax to equilibrium, due to an increased structuring of the interface with a commensurate viscoelastic response. The insert in Figure 7 (A) shows the evolution of the relaxation time, as obtained from fitting the relaxation following each step compression, for different compression speeds (as illustrated in Supplementary Figure S.1.-S.2.).

For an apparent isotherm measured at constant speed, the strain rate will vary over the measurement and it is calculated as:

$$\dot{\lambda} = 2\frac{\Delta D(t)}{\Delta t}\frac{1}{D(t)} \tag{31}$$

where $D(t)$ is the trough diameter as a function of time and $\Delta D/\Delta t$ represents the constant compression speed. The reciprocal of this strain rate is taken as the so called characteristic time of observation[59]. Comparing this time of observation with the viscoelastic relaxation time τ of the actual system, the non-dimensional Deborah number can be defined[60]:

$$De = \frac{\tau}{\lambda} \tag{32}$$

Figure 7 (B) shows the evolution of the Deborah number (De) for the present system during a compression measurement with a speed of 1.5 mm/min. It can be seen that De increases as the interface becomes increasingly viscoelastic, and will turn into a solid material at high compression ratios. For $De > 1$ strong viscoelastic effects are expected. The measured surface pressure will then contain rheological contributions. As long as the relaxation time is finite, these effects can be separated out by allowing the interface to relax. However, when a solid state is achieved, these extra stresses will remain present, commensurate with a solid elastic response. Therefore, rheological effects inevitably influence what is invariably called a "pressure-area isotherm", and this is a general result for all insoluble monolayers which eventually form solid-like or highly structured phases. For this reason we prefer to refer to these curves as an "apparent" isotherm.In the current case, De starts to increase significantly for densities above 15 Å^2 per molecule, leading us to propose to use this surface density as the start of the strongly elastic regime.
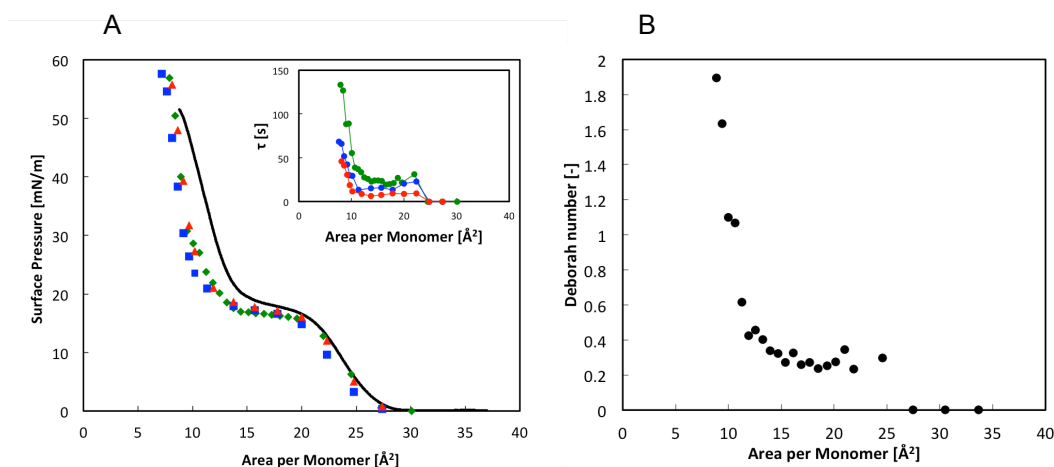
Fig. 7 Results of the stepwise compression measurements. (A) Apparent surface pressure obtained during continuous (black line, 1.5 mm/min) and stepwise compression measurements (colored symbols) versus area per monomer (compression speeds prior to relaxation: 1.5 mm/min (green symbols), 7 mm/min (blue symbols) and 20 mm/min (red symbols)). The inset shows the relaxation times τ as a function of the area per monomer (B): Evolution of the Deborah number for a compression speed of 1.5 mm/min.
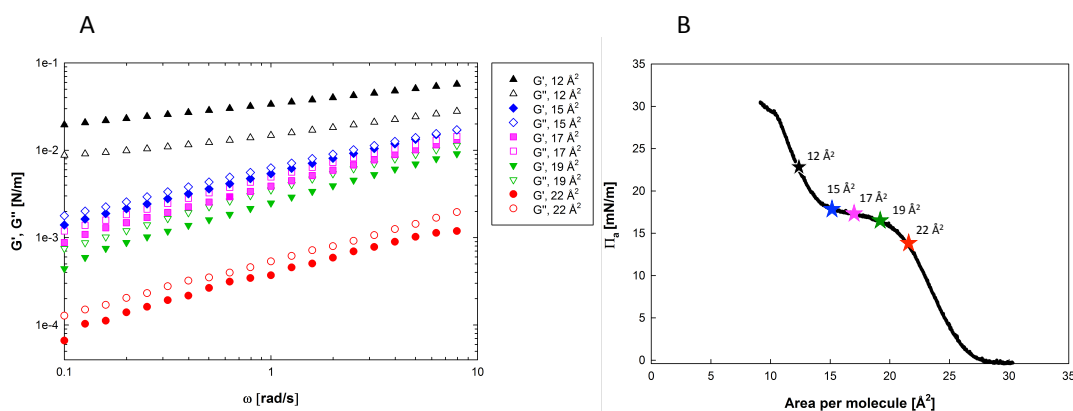

Fig. 8 Results of interfacial shear rheology. (a) Linear viscoelastic shear moduli as a function of frequency for PtBMA at the air-water interface at strain amplitude of 1%. (b) Apparent surface pressure as a function of surface coverage during the shear measurements.

4.3 Linear viscoelastic properties

In order to relate the change in behaviour of this system at 15 Å^2 to its micro-structural modifications, interfacial shear rheology was measured at controlled surface pressures. Shear rheometry only picks up the material properties corresponding to the deviatoric stresses and hence is maybe better suited to interrogate the interfacial microstructure. In Figure 8 the results of frequency sweeps at different values of compression ratios in the linear viscoelastic regime are shown. As long

as the monolayer is kept in the liquid expanded state (Areas per monomer 22, 19 and 17 Å^2) the frequency dependent response of PtBMA shows a predominantly liquid viscoelastic behaviour with G''_s consistently higher than G'_s. When the layer is compressed past the critical value of 15 Å^2, a gradual and continuous transition from predominantly viscous to a more elastic behaviour is observed. These findings confirm the divergence of the relaxation time in the measured isotherms as being due to the development of increasingly

elastic layers, in agreement with earlier work[51].

5 Finite strain constitutive model for elastic interfaces

In the present work, three experimental techniques are used to evaluate the mechanical response of an elastic interface: the Langmuir trough, the radial trough and shear rheometry in the linear viscoelastic limit. The goal is to exploit the observations in the solid, elastic regime and use these data to evaluate the quasi linear constitutive equations. However, to experimentally determine elastic deformations, first a reference configuration must be defined. In the previous section it was established experimentally by the evolution of the linear viscoelastic shear properties, that at packing densities below 15 Å² per molecule, the PtBMA layer at an air-water interface starts to behave elastically, identified as the point where De started to increase significantly in Figure 7 (B). For compression experiments in both the Langmuir and the radial trough, a surface concentration of 15 Å² per molecule is chosen as stress-free reference configuration, where $\lambda_1^* = J = 1$ and $\boldsymbol{\sigma}^e = \mathbf{0}$. In other words, it is assumed that upon compressing the PtBMA layer to a value of $x < 15$ Å² per molecule, the relative area deformation J in the radial trough equals: $J = x/15$. In the Langmuir trough, the same compression gives $\lambda = J = x/15$.
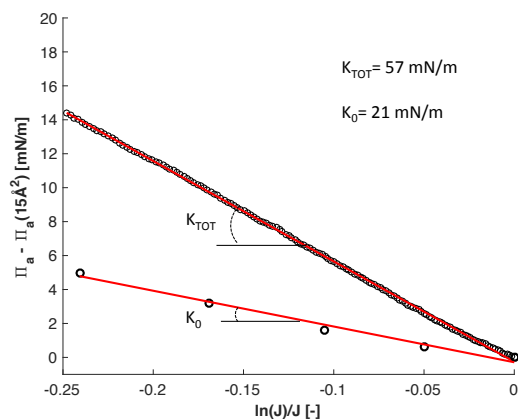

Fig. 9 Normalized surface pressure as a function of $\ln(J)/J$ during compression in the radial trough for both the continuous compression (1.5 mm/min, upper curve) and the data obtained from the stepwise experiments (lower curve). The slope of the straight line equals the surface-dilatational modulus K and was found to be $K_{TOT} = 57$ mN/m for the response upon continuous compression and $K_0 = 21$ mN/m for the data obtained from the static curve.

As was shown in section 2, for the radial trough,

the isotropic part of the extra stress σ_e^{iso} is governed by the Hencky-strain measure $\ln(J)/J$ as: $\sigma_1 = \sigma_2 = \sigma_e^{iso} = K\ln(J)/J$ (see Equation 22). From this it follows that a plot of σ_e^{iso} versus $\ln(J)/J$ should give a straight line with a slope equal to the surface-dilatational modulus K, as is shown in Figure 9. Approximating the total isotropic elastic stress σ_e^{iso} by the increase in the apparent surface pressure (normalized with respect to the value at 15 Å² per molecule) in the radial through, Equation (22) is observed to accurately describe the isotropic-stress response up to $\ln(J)/J = -0.25$, corresponding to an area change of approximately 20%. From the linear fit, the effective surface-dilatational modulus K_{TOT} from the continuous compression experiment was found to be $K = 57$ mN/m. It should be noted that the K_{TOT} value obtained in this way, by using the increase in the apparent surface pressure, contains both the static elasticity (related to the inherent compressibility) and the extra elastic stresses. Hence K_{TOT} represents an apparent modulus containing effects of the compressibility, the elastic and the viscoelastic response. The static data of Figure 7 (A) for the surface pressure after relaxation, can also be described very well by the neo-Hookean model as is shown by the lower curve in Figure 9. The static modulus equals $K_0 = 21$ mN/m and reflects the thermodynamic compressibility (changes in Γ lead to changes in $\sigma_{\alpha\beta}$) and possibly other static contributions, such as those from solid like features in the spread glassy polymer layer. The observed behaviour with $K_{TOT} > K_0$ is be a consequence of the specific microstructure of the PtBMA monolayers obtained after spreading. Would it be possible to generate different unstrained reference states, for example, by different spreading or specific adsorption protocols, these effects could be further de-convoluted. In the present case for the PtBMA, this was not possible as spreading in the regime where multilayered structures are observed may lead to different structures compared to structures obtained by compression. The system is characterised by extra stresses, and the Neo-Hookean model fits both the static and continuous compression data very good.

Furthermore, the Neo-Hookean model predicts that the normal-stress difference $(\sigma_1 - \sigma_2)$, as measured by two Wilhelmy plates, placed perpendicular with respect to each other in a Langmuir trough (see Figure 5), only depends on the surface shear modulus G as: $(\sigma_1 - \sigma_2) = G\left(1 - 1/\lambda^2\right)$, see Equation (18a). This was verified experimentally as shown in Figure 10. As can be seen in this figure, the normal stress difference is well described by the Neo-Hookean relation up to a strain of $(1 - 1/\lambda^2) = -0.5$, corresponding to a compression of approximately 30%. From the linear fit, the surface shear modulus G was found to be $G = 24$ mN/m. This value for G compares well with the values obtained for the dynamic shear modulus as found by interfacial shear rheology
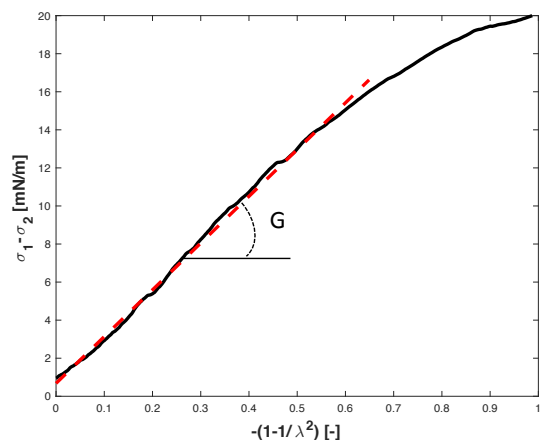
Fig. 10 The normal stress difference $(\sigma_1 - \sigma_2)$ as a function of $(1 - 1/\lambda^2)$. The slope of the straight line equals the surface-shear modulus G and was found to be $G = 24$ mN/m.

(see Figure 8). As the normal-stress difference response in a Langmuir trough as predicted by the Hencky-strain model is almost indistinguishable from that of the Neo-Hookean model (see Figure 2), the Hencky-strain plot is not shown.

The fitted values of K_{TOT} and G can now be used to predict the full extra-stress response (σ_1 and σ_2) in a Langmuir trough using the Neo-Hookean model (Equation (21)). This is shown together with the experimental curves in Figure 11. Here, it can be seen that the experimental elastic response is well described by the theoretical predictions for deformations up to about 20%, confirming that the response of these glassy polymer layers are dominated by the extra stresses, as was also shown by the shear rheological data of Figure 8.

The quasilinear model presented here is a step towards more elaborate rheological models. A simple extension is to make the material parameters time dependent. For the shear modulus this is straightforward ($G(t)$). For the compression modulus, the static modulus will however be time-independent, and only the extra elastic stresses should be considered ($(K_{TOT} - K_0)(t)$) . Further nonlinear material functions can be introduced, similar as has been done for bulk rheology [13].

The analysis shown in the present work shows that measurements using a Langmuir-Pockels rectangular trough should be interpreted carefully, in particular when dense structured phases are encountered. In the present work a polymer layer was selected wheree the transition from when thermodynamic transport phenomena govern interfacial properties into the region where rheological effects are dominant
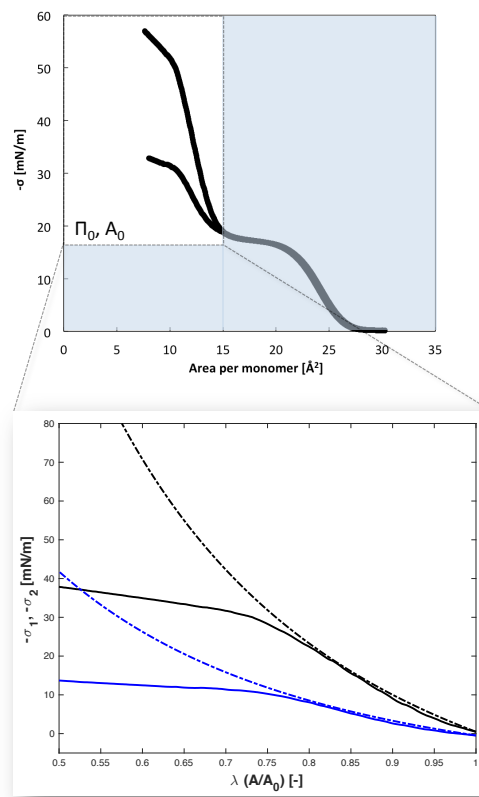

Fig. 11 The negative principle extra surface stresses $-\sigma_1$ and $-\sigma_2$ (insert) in relation to the total pressure-area isotherm. The black lines correspond to $-\sigma_1$ and the blue lines to $-\sigma_2$. The solid lines are the experimental curves and the dashed lines are the predictions using Equation (21).

was rather abrupt. Often, such an evolution will be much more gradual. To obtain insight into the repsonse measured it may be important to independently measure the shear rheological properties, because as soon as a significant shear elasticity is measured, there will be sufficient microstructure present, to also expect a significant mechanical response in compression. Second, a simple guideline is that thermodynamic properties are dependent on the state of the system alone, and are hence independent of geometry and strain history, whereas the mechanical response will be dependent on strain and straining direction. Finally, stepwise experiments as in figure 7 provide guidance in identifying equilibrium properties, but there also transport phenomena to and from the interface should be considered (which will also depend on geometry, see Alvarez et al. [61]).

6 Conclusions

For complex fluid-fluid interfaces, a constitutive relation between the surface-stress tensor and the strains is required. The generalisation of rheological models from bulk fluids is not trivial, as interfaces are generally compressible and the dilational/compressional aspects need to be considered. In the present work, a constitutive model for finite elastic deformations of the interface was derived from a strain energy function. This interfacial "neo-Hookean" constitutive equation can be written in a coordinate-free tensor form and separates the dilatational/compressional contributions from the contributions related to shear deformations. To test the model, PtBMA layers were selected, as they were expected to display this neo-Hookean behaviour when compressed to small enough mean molecular areas. These layers were tested in different geometries, including shear flow, homogeneous isotropic compression using a radial though and homogeneous compression using a standard Langmuir though. The radial-ribbon through is designed for precise rheological studies in compression. Using stepwise compression experiments, the conditions where the neo-Hookean behaviour is expected to occur were identified, and the value of the compression modulus during continuous compression was determined. The shear modulus was independently measured using a shear rheometer with double wall ring geometry. These shear measurements as function of surface pressure showed a pronounced shear elasticity once the layer is compressed to high surface pressures. The model in combination with the independently measured compression and shear moduli can the be used to predict the dependence of the experimentally determined surface pressure on the orientation of the Wilhelmy plate up to strains of 20%. Finally, it should be noted that all measurements were performed at relatively high Deborah numbers, considering only a single loading path in compression at constant strain rate. The compression moduli during stepwise compression are lower and reflect better the static elasticity and compressibility of the quiescent structure obtained after spreading. The continuous compression experiment represented a fast deformation of a viscoelastic interface and enhanced the effects of the extra stresses.

As for bulk materials, the model is an important building block for non-linear rheological models which are intended to describe the extra and deviatoric stresses. It is also important to recognise that in phase diagram studies, when solid or highly structured phases are studied, the time scale of the deformation during the compression will be faster than the relaxation times of the interface, leading to an elastic response. All phase diagram studies and investigations of phase changes with Langmuir monolayers should be performed with the possibility in mind that extra and deviatoric stresses may be present, which will be recorded together with changes of the thermodynamic state variables. Constitutive models, in combination with thermodynamic models or measurements with different geometries, such as those presented here, should enable us to de-convolute these different effects or identify conditions where one or the other dominates.

References

1 G. G. Fuller and J. Vermant, "Complex Fluid-Fluid Interfaces: Rheology and Structure," *Annual Review of Chemical and Biomolecular Engineering*, vol. 3, no. 1, pp. 519–543, 2012.

2 L. M. C. Sagis, "Dynamic properties of interfaces in soft matter: Experiments and theory," *Reviews of Modern Physics*, vol. 83, no. 4, pp. 1367–1403, 2011.

3 P. Erni, "Deformation modes of complex fluid interfaces," *Soft Matter*, vol. 7, no. 17, pp. 7586–7600, 2011.

4 D. Langevin, "Influence of interfacial rheology on foam and emulsion properties," *Advances in Colloid and Interface Science*, vol. 88, no. 1-2, pp. 209–222, 2000.

5 E. Hermans, M. Saad Bhamla, P. Kao, G. G. Fuller, and J. Vermant, "Lung surfactants and different contributions to thin film stability," *Soft Matter*, vol. 11, no. 41, pp. 8048–8057, 2015.

6 E. Hermans and J. Vermant, "Interfacial shear rheology of DPPC under physiologically relevant conditions.," *Soft Matter*, vol. 10, no. 1, pp. 175–186, 2014.

7 D. Halpern, H. Fujioka, S. Takayama, and J. B. Grotberg, "Liquid and surfactant delivery into pulmonary airways," *Respiratory Physiology and Neurobiology*, vol. 163, no. 1-3, pp. 222–231, 2008.

8 R. Pattle, "Properties, function and origin of the alveolar lining layer.," *Nature*, vol. 175, pp. 1125–1126, 1955.

9 C. Alonso, T. Alig, J. Yoon, F. Bringezu, H. Warriner, and J. A. Zasadzinski, "More than a monolayer: relating lung surfactant structure and mechanics to composition.," *Biophys J*, vol. 87, no. 6, pp. 4188–4202, 2004.

10 M. S. Bhamla, C. E. Giacomin, C. Balemans, and G. G. Fuller, "Influence of interfacial rheology on drainage from

curved surfaces," *Soft Matter*, vol. 10, no. 36, pp. 6917–6925, 2014.

11 W. Sempels, R. De Dier, H. Mizuno, J. Hofkens, and J. Vermant, "Auto-production of biosurfactants reverses the coffee ring effect in a bacterial system.," *Nature communications*, vol. 4, p. 1757, 2013.

12 T. Verwijlen, L. Imperiali, and J. Vermant, "Separating viscoelastic and compressibility contributions in pressure-area isotherm measurements," *Advances in Colloid and Interface Science*, vol. 206, pp. 428–436, 2014.

13 C. Macosko, *Rheology: Principles, Measurements and Applications.* No. 3, Wiley-VCH, 1996.

14 V. Kovalchuk, R. Miller, V. Fainerman, and G. Loglio, "Dilational rheology of adsorbed surfactant layers, role of the intrinsic two-dimensional compressibility," *Advances in Colloid and Interface Science*, vol. 114-115, pp. 303 – 312, 2005.

15 J. Lucassen and M. V. D. Tempel, "Dynamic measurements of dilational properties of a liquid interface," *Chemical Engineering Science*, vol. 27, no. 6, pp. 1283 – 1291, 1972.

16 M. D. Reichert, N. J. Alvarez, C. F. Brooks, A. M. Grillet, L. A. Mondy, S. L. Anna, and L. M. Walker, "The importance of experimental design on measurement of dynamic interfacial tension and interfacial rheology in diffusion-limited surfactant systems," *Colloids and Surfaces A: Physicochemical and Engineering Aspects*, vol. 467, pp. 135–142, 2015.

17 S. Reynaert, C. F. Brooks, P. Moldenaers, J. Vermant, and G. G. Fuller, "Analysis of the magnetic rod interfacial stress rheometer," *Journal of Rheology*, vol. 52, no. 1, pp. 261–285, 2008.

18 P. Erni, P. Fischer, E. J. Windhab, V. Kusnezov, H. Stettin, and J. Läuger, "Stress- and strain-controlled measurements of interfacial shear viscosity and viscoelasticity at liquid/liquid and gas/liquid interfaces," *Review of Scientific Instruments*, vol. 74, no. 11, pp. 4916–4924, 2003.

19 S. Vandebril, A. Franck, G. G. Fuller, P. Moldenaers, and J. Vermant, "A double wall-ring geometry for interfacial shear rheometry," *Rheologica Acta*, vol. 49, no. 2, pp. 131–144, 2010.

20 S. Fitzgibbon, E. S. G. Shaqfeh, G. G. Fuller, and T. W. Walker, "Scaling analysis and mathematical theory of the interfacial stress rheometer," *Journal of Rheology*, vol. 58, no. 4, pp. 999–1038, 2014.

21 O. H. Soo-Gun and J. C. Slattery, "Disk and biconical interfacial viscometers," *Journal of Colloid And Interface Science*, vol. 67, no. 3, pp. 516–525, 1978.

22 C. F. Brooks, G. G. Fuller, C. W. Frank, and C. R. Robertson, "Transitions in Monolayers at the Air - Water Interface," *Langmuir*, vol. 5, no. 14, pp. 2450–2459, 1999.

23 P. A. Rühs, N. Scheuble, E. J. Windhab, R. Mezzenga, and P. Fischer, "Simultaneous control of ph and ionic strength during interfacial rheology of β-lactoglobulin fibrils adsorbed at liquid/liquid interfaces," *Langmuir*, vol. 28, no. 34, pp. 12536–12543, 2012.

24 B. Schroyen, D. Z. Gunes, and J. Vermant, "A versatile subphase exchange cell for interfacial shear rheology," *Rheologica Acta*, vol. 56, no. 1, pp. 1–10, 2017.

25 D. B. Jones and A. P. J. Middelberg, "Direct determination of the mechanical properties of an interfacially adsorbed protein ÿlm," *Chemical Engineering Science*, vol. 57, pp. 1711–1722, 2002.

26 T. Verwijlen, D. L. Leiske, P. Moldenaers, J. Vermant, and G. G. Fuller, "Extensional rheometry at interfaces: Analysis of the Cambridge Interfacial Tensiometer," *Journal of Rheology,*, vol. 56, no. 5, pp. 1225–1247, 2012.

27 J. T. Petkov, T. D. Gurkov, B. E. Campbell, and R. P. Borwankar, "Dilatational and shear elasticity of gel-like protein layers on air/water interface," *Langmuir*, vol. 16, no. 8, pp. 3703–3711, 2000.

28 E. Aumaitre, D. Vella, and P. Cicuta, "On the measurement of the surface pressure in Langmuir films with finite shear elasticity," *Soft Matter*, vol. 7, no. 6, pp. 2530–2537, 2011.

29 P. Cicuta and D. Vella, "Granular character of particle rafts," *Physical Review Letters*, vol. 102, no. 13, pp. 1–4, 2009.

30 K. Halperin, J. B. Ketterson, and P. Dutta, "A Study of The Mechanical Behavior of Surface Monolayers Using Orthogonal Wilhelmy Plates," *Langmuir*, vol. 5, no. 1, pp. 161–164, 1989.

31 N. A. Alexandrov, K. G. Marinova, T. D. Gurkov, K. D. Danov, P. A. Kralchevsky, S. D. Stoyanov, T. B. Blijdenstein, L. N. Arnaudov, E. G. Pelan, and A. Lips, *Interfacial layers from the protein HFBII hydrophobin: Dynamic surface tension, dilatational elasticity and relaxation times*, vol. 376. Elsevier, 2012.

32 A. A. Badran and E. Marschall, "Oscillating pendant drop: A method for the measurement of dynamic surface and interface tension," *Review of Scientific Instruments*, vol. 57, no. 2, pp. 259–263, 1986.

33 H.-J. Butt, K. Graf, and M. Kappl, "Physics and Chemistry of Interfaces," *Wiley-VCH*, pp. 118–144, 2003.

34 K. D. Danov, R. D. Stanimirova, P. A. Kralchevsky, K. G. Marinova, N. A. Alexandrov, S. D. Stoyanov, T. B. J. Blijdenstein, and E. G. Pelan, "Capillary meniscus dynamometry - Method for determining the surface tension of drops and bubbles with isotropic and anisotropic surface stress distributions," *Journal of Colloid and Interface Science*, vol. 440, pp. 168–178, 2015.

35 S. Knoche, D. Vella, E. Aumaitre, P. Degen, H. Rehage, P. Cicuta, and J. Kierfeld, "Elastometry of deflated cap-

sules: Elastic moduli from shape and wrinkle analysis," *Langmuir*, vol. 29, no. 40, pp. 12463–12471, 2013.

36 M. Nagel, T. A. Tervoort, and J. Vermant, "From drop-shape analysis to stress-fitting elastometry," *Advances in Colloid and Interface Science*, pp. –, 2017.

37 A. P. Kotula and S. L. Anna, "Regular perturbation analysis of small amplitude oscillatory dilatation of an interface in a capillary pressure tensiometer," *Journal of Rheology*, vol. 59, no. 1, pp. 85–117, 2015.

38 G. Enhorning, "Pulsating bubble technique for evaluating pulmonary surfactant.," *Journal of Applied Physiology*, vol. 43, no. 2, pp. 198–203, 1977.

39 B. M. Abraham, K. Miyano, S. Q. Xu, and J. B. Ketterson, "Centro-symmetric technique for measuring shear modulus, viscosity, and surface tension of spread monolayers," *Review of Scientific Instruments*, vol. 54, no. 2, pp. 213–219, 1983.

40 K. Miyano and T. Maeda, "Langmuir trough with four movable barriers," *Review of Scientific Instruments*, vol. 58, no. 3, pp. 428–435, 1987.

41 T. M. Bohanon, J. B. Ketterson, and P. Dutta, "Surface Tension Anisotropy and Relaxation in Uniaxially Compressed Langmuir Monolayers," *Langmuir*, no. 8, pp. 2497–2500, 1992.

42 M. Matsumoto, Y. Tsujii, K.-I. Nakamura, and T. Yoshimoto, "A trough with radial compression for studies of monolayers and fabrication of Langmuir-Blodgett films," *Thin Solid Films*, vol. 280, no. 1-2, pp. 238–243, 1996.

43 C. Balemans, M. A. Hulsen, T. A. Tervoort, and P. D. Anderson, "Erratum to: Modeling of complex interfaces for pendant drop experiments," *Rheologica Acta*, vol. 56, no. 6, pp. 597–599, 2017.

44 C. Truesdell and W. Noll, "The non-linear field theories of mechanics," in *The non-linear field theories of mechanics*, pp. 1–579, Springer, 2004.

45 R. W. Ogden, "on the Thermoelastic Modeling of Rubber-like Solids," *Journal of Thermal Stresses*, vol. 15, no. 4, pp. 533–557, 1992.

46 R. Anand, "On H. Hencky's approximate strain-energy function for moderate deformations," *Journal of Applied Mechanics*, vol. 46, pp. 78–82, 1979.

47 M. Hutter and T. A. Tervoort, "Thermodynamic considerations on non-isothermal finite anisotropic elasto-viscoplasticity," *Journal of Non-Newtonian Fluid Mechanics*, vol. 152, no. 1-3, pp. 53–65, 2008.

48 J. E. Fitzgerald, "A tensorial Hencky measure of strain and strain rate for finite deformations," *J. Appl. Phys.*, vol. 51, no. 10, pp. 5111–5115, 1980.

49 P. Gijsenbergh, M. Pepicelli, C. L. Wirth, J. Vermant, and R. Puers, "Langmuir monolayer characterization via polymer microtensiometers," *Sensors and Actuators, A: Physical*, vol. 229, pp. 110–117, 2015.

50 Z. A. Zell, S. Q. Choi, L. G. Leal, and T. M. Squires, "Microfabricated deflection tensiometers for insoluble surfactants," *Applied Physics Letters*, vol. 97, no. 13, pp. 1–4, 2010.

51 G. T. Gavranovic, J. M. Deutsch, and G. G. Fuller, "Two-Dimensional Melts: Polymer Chains at the Air-Water Interface," *Macromolecules*, vol. 38, no. 15, pp. 6672–6679, 2005.

52 A. Maestro, L. J. Bonales, H. Ritacco, T. M. Fischer, R. G. Rubio, and F. Ortega, "Surface rheology: macro-and microrheology of poly (tert-butyl acrylate) monolayers," *Soft Matter*, vol. 7, no. 17, pp. 7761–7771, 2011.

53 S. Srivastava, D. Leiske, J. K. Basu, and G. G. Fuller, "Interfacial shear rheology of highly confined glassy polymers," *Soft Matter*, vol. 7, pp. 1994–2000, 2011.

54 Y.-K. See, J. Cha, T. Chang, and M. Ree, "Glass transition temperature of poly(tert-butyl methacrylate) langmuir-blodgett film and spin-coated film by x-ray reflectivity and ellipsometry," *Langmuir*, vol. 16, no. 5, pp. 2351–2355, 2000.

55 P. Sollich, F. m. c. Lequeux, P. Hébraud, and M. E. Cates, "Rheology of soft glassy materials," *Physical Review Letters*, vol. 78, pp. 2020–2023, Mar 1997.

56 P. Cicuta and E. M. Terentjev, "Viscoelasticity of a protein monolayer from anisotropic surface pressure measurements," *European Physical Journal E*, vol. 16, no. 2, pp. 147–158, 2005.

57 M. Sacchetti, H. Yu, and G. Zografi, "In-plane steady shear viscosity of monolayers at the air/water interface and its dependence on free area," *Langmuir*, vol. 9, no. 8, pp. 2168–2171, 1993.

58 G. T. Gavranovic, M. M. Smith, W. Jeong, A. Y. Wong, R. M. Waymouth, and G. Fuller, "Effects of temperature and chemical modification on polymer Langmuir films.," *The Journal of Physical Chemistry. B*, vol. 110, no. 44, pp. 22285–90, 2006.

59 T. Kato, "What Is the Characteristic Time of Measurement of pressure-area Isotherms? Necessity of a Constant Strain Rate of Compression of Insoluble Monolayers for pressure-area Measurements," *Langmuir*, no. 6, pp. 870–872, 1990.

60 M. Reiner, "The Deborah Number," *Physics Today*, vol. 17, no. 1, p. 62, 1964.

61 N. J. Alvarez, L. M. Walker, and S. L. Anna, "A microtensiometer to probe the effect of radius of curvature on surfactant transport to a spherical interface," *Langmuir*, vol. 26, no. 16, pp. 13310–13319, 2010.